Electronic Supplementary Information (ESI)

Neuromorphic devices realised using Self-Forming Hierarchical Al and Ag Nanostructures: Towards Energy-Efficient, wide ranging Synaptic Plasticity

Rohit Attri,[a] *Indrajit Mondal,*[b] *Bhupesh Yadav,*[b] *G. U. Kulkarni,*[b]* and *C. N. R. Rao*[a, b]

[a] New Chemistry Unit, and School of Advanced Materials (SAMat), Jawaharlal Nehru Centre for Advanced Scientific Research, Bangalore-560064, India.

[b] Chemistry and Physics of Materials Unit and School of Advanced Materials (SAMat), Jawaharlal Nehru Centre for Advanced Scientific Research, Bangalore-560064, India.

*Corresponding author, Email: kulkarni@jncasr.ac.in

Figure S1: Optical images of the c-Al fabrication process taken after (a) crack precursor (CP) coating on Al thin film deposited glass substrate, (b) baking of CP coated substrate at 150 ºC for 10 min, (c) etching of underlying Al film through the interconnected micro-gaps created by CP self-drying. All images are taken in reflection geometry. Compare the images, the networked gap closely resembles the crack pattern. Scale bar, 200 µm.

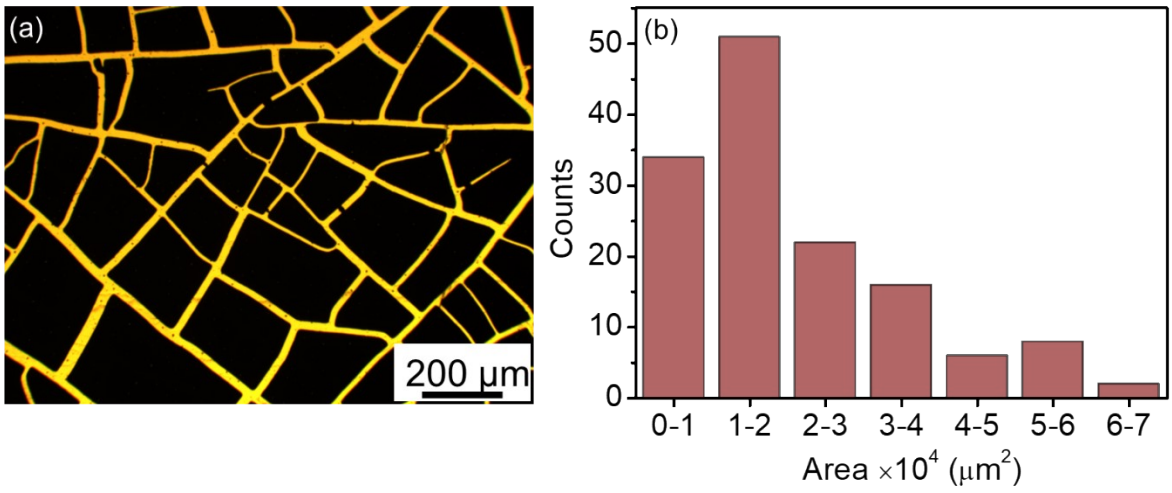

Figure S2: (a) The optical image (transmission mode) of c-Al having Al two-dimensional fill factor of 79.6 %. (b) Histogram showing the size distribution of Al islands. Many islands are in the range of 1-2 × 10^4 µm^2 while the average value is 2.14 × 10^4 µm^2. (For accuracy, Al islands on the edge were excluded)

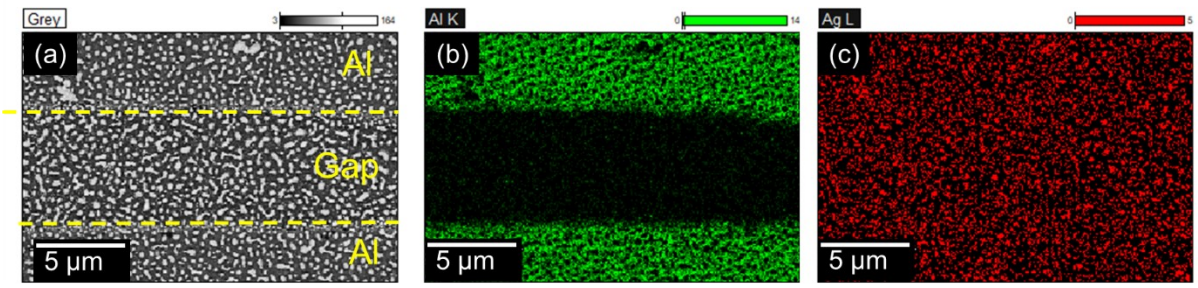

Figure S3: (a) FESEM image and EDS maps (b and c) of a device. The absence of Al K signal in the micro-gap may be noted. Ag L is seen all over the device is expected from the deposition.

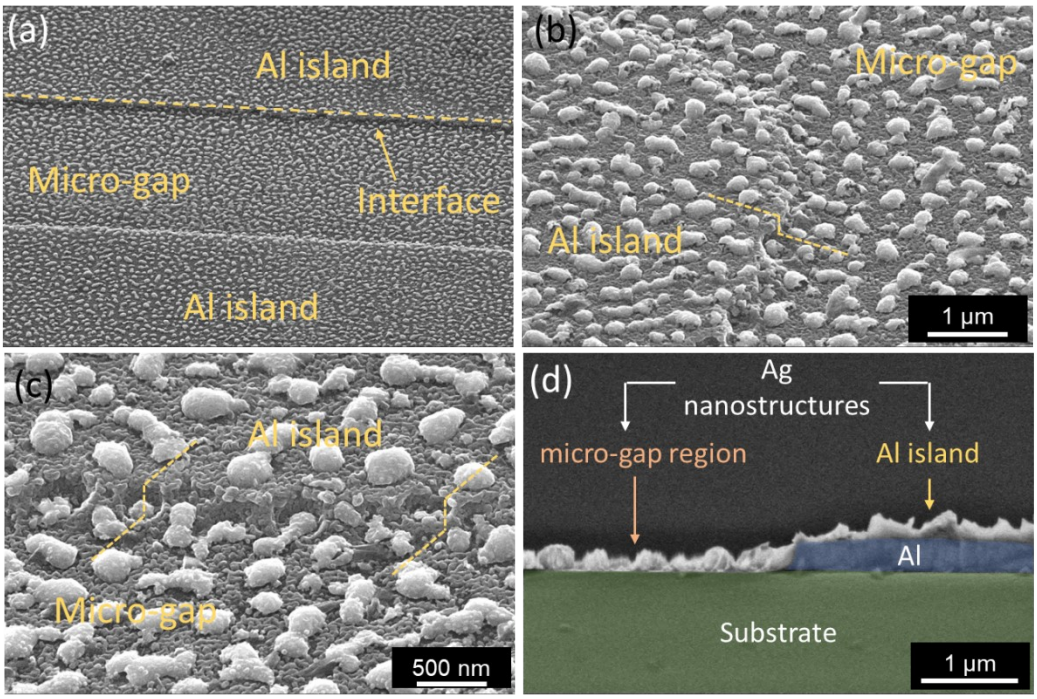

Figure S4: (a-c) Plane view FESEM images captured with the tilt angle of 52° of c-Al highlighting Ag nanostructures interlacing at the interface of Al island and micro-gap region. (dashed line indicates the step) (d) cross-sectional FESEM image of the c-Al with Ag nanostructures on Al island (thickness ~ 215 nm) and in the micro-gap. (False colors are used to highlight the interfaces)

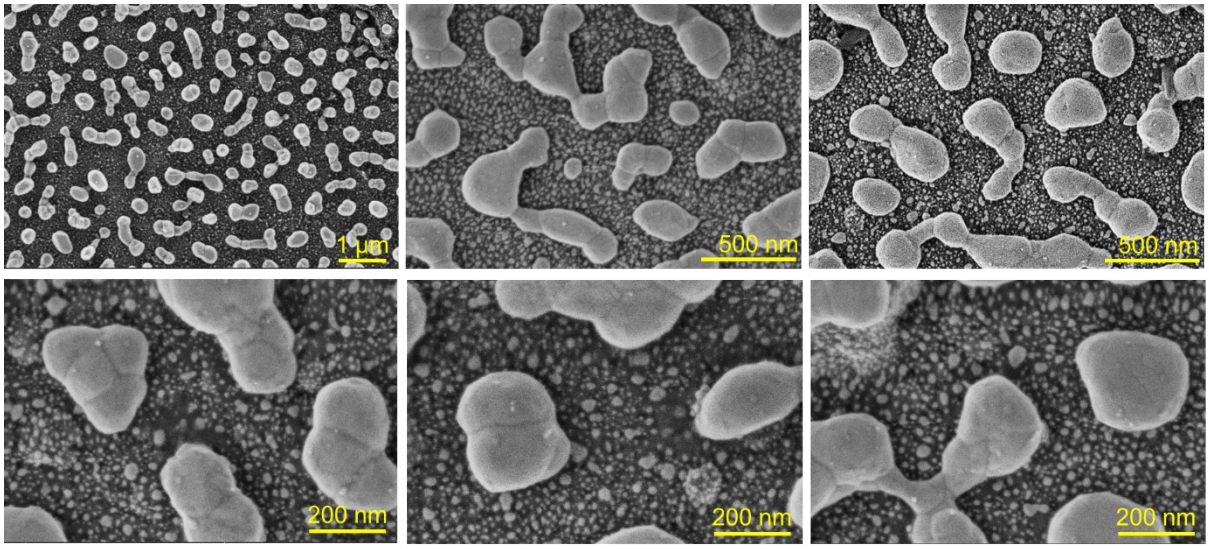

Figure S5: FESEM images collected from different regions in the micro-gap of the device. The hierarchical nature of the Ag nanostructures is evident in all areas.

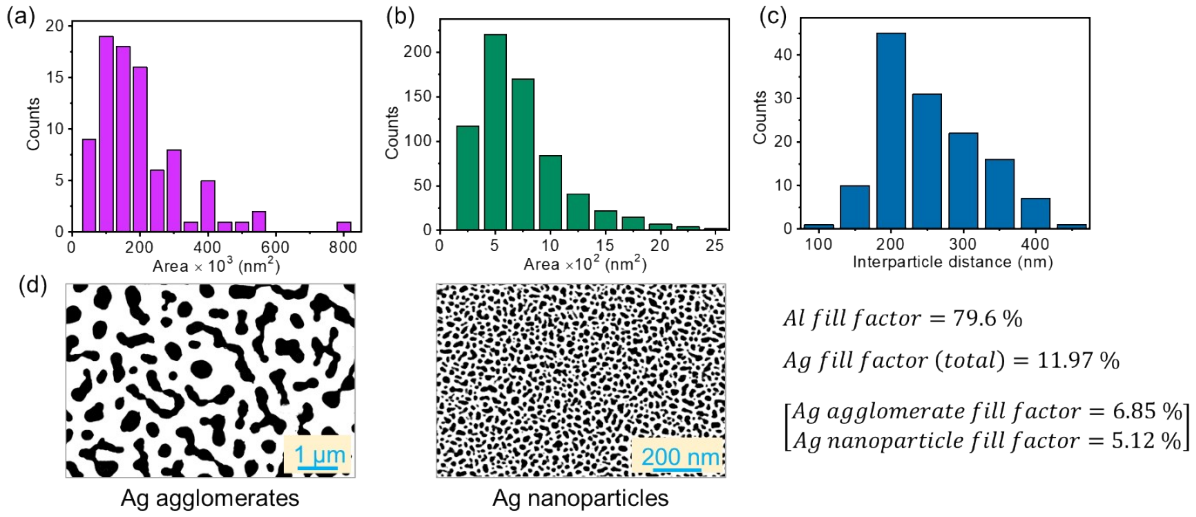

Figure S6: Detailed coverage analysis and size distribution histogram of Ag nanostructures, (a) agglomerates and (b) nanoparticles in the micro-gap of the c-Al with average size of ~ 171 × 10^3 nm^2, and ~ 589 nm^2, respectively. The average diameter of nanoparticle is ~ 27 nm. (c) Inter-agglomerate distance distribution histogram. The average distance between nearest neighbours is ~ 227 nm. (d) 2D fill factor calculated from the FESEM binary image of Ag agglomerates and nanoparticles.

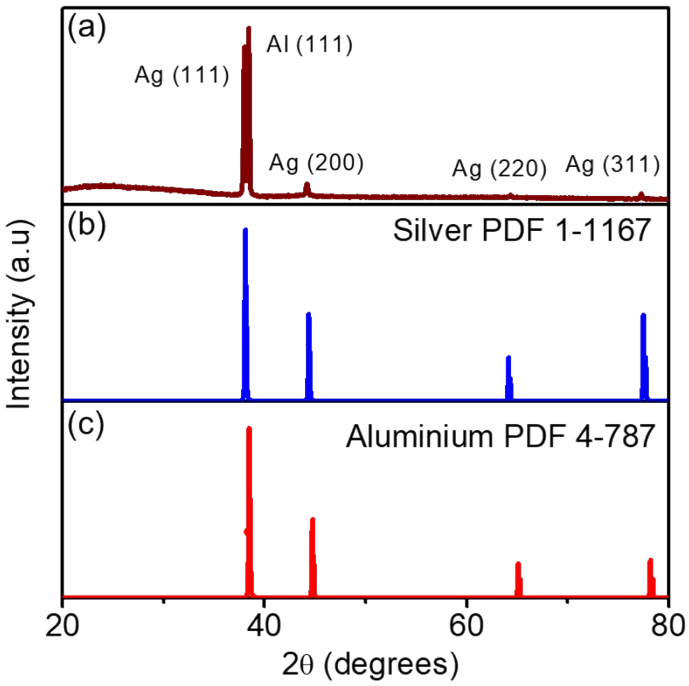

Figure S7: (a) XRD pattern showing Al(111) peak of c-Al, and polycrystalline nature of Ag nanostructures with multiple crystallographic reflections probably due to their morphology. No oxide phase is observed post the fabrication process. Simulated pattern of (b) Ag, and (c) Al.

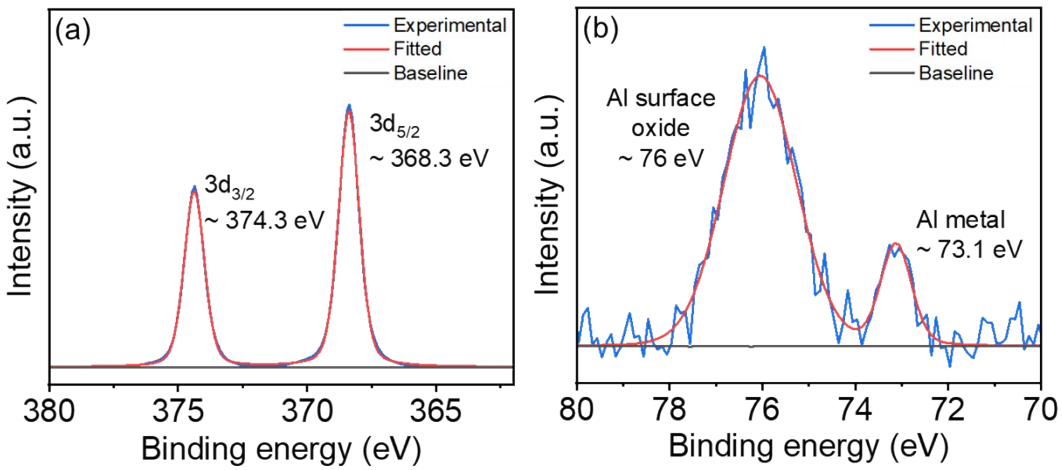

Figure S8: Core level X-ray photoelectron (XP) spectra of (a) Ag 3d, and (b) Al 2p showing the chemical nature of hierarchical Al and Ag structures. Slight blueshift in Al 2p binding energy could be due to sample charging during surface cleaning.

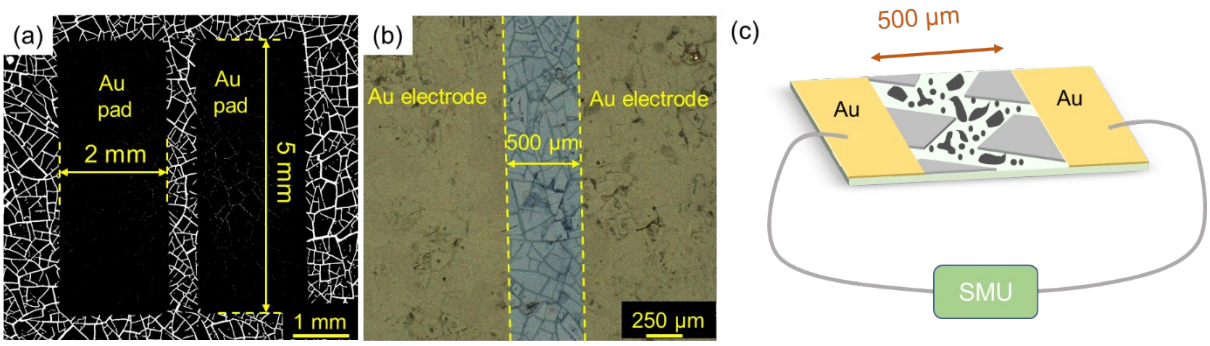

Figure S9: (a) Optical image of the Au contact pads as electrodes having dimensions of 5 mm × 2 mm (transmission mode), (b) magnified optical image showing the electrodes separated with the gap of 500 µm (reflection mode), (c) schematic showing the fabricated c-Al with Ag nanostructures device connected to SMU for electrical measurements.

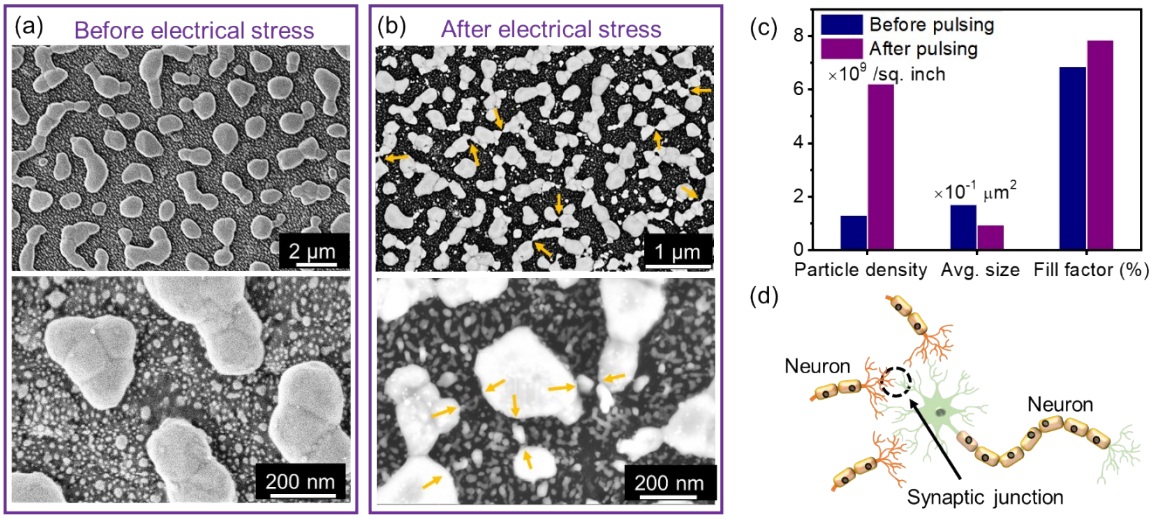

Figure S10: FESEM images of the device before (a), and after (b) electrical voltage sweeping. Images at high magnification (bottom panel) illustrate the appearance of filamentary growths under electrical stress. See arrows mark regions as examples. (c) Histogram showing variation of parameters of Ag nanostructures after the electrical stress on the device. (d) Schematic of biological synaptic network, which could be correlated with nanogaps in between agglomerates shown in (a) and (b).

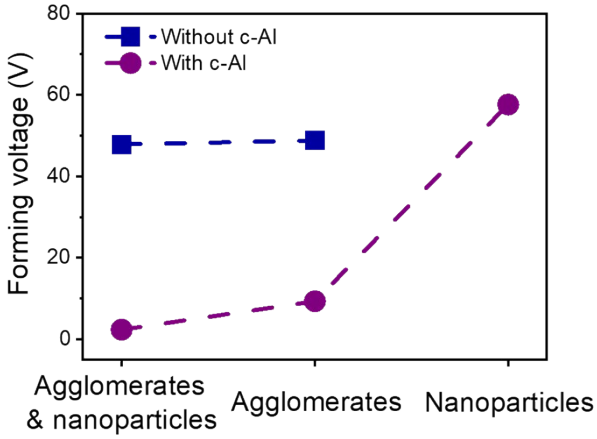

Figure S11: Forming voltage derived data from I-V characteristics of ASN devices of different configurations with and without c-Al, respectively.

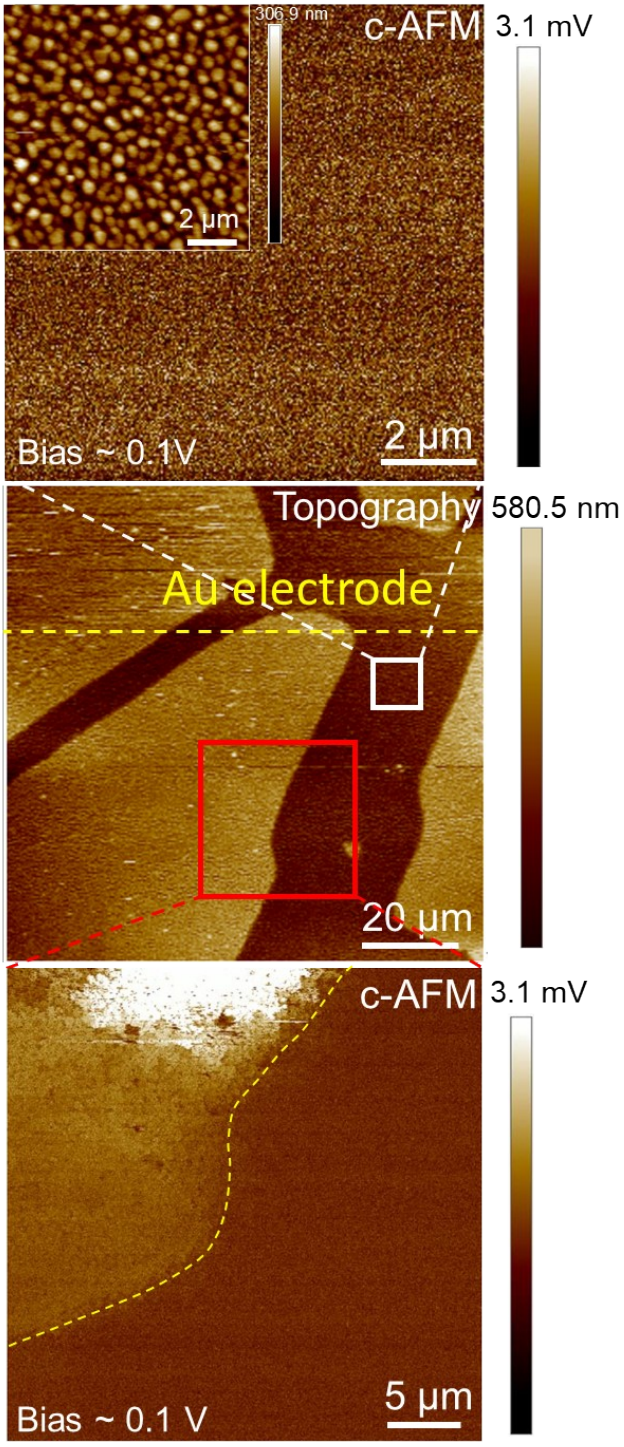

Figure S12: Contact mode AFM image (middle) of device D1 in HRS near the Au electrode (marked with yellow dashed line). Conductive AFM (c-AFM) signal recorded in HRS at the tip bias voltage of 0.1 V w.r.t the ground Au electrode. c-AFM image (top) shows low output voltage from the area pertaining to Ag nanostructures in the micro-gap region indicating no percolation path in HRS of device (Inset shows topography AFM image with the avg. surface roughness ~ 43 nm). In contrast the c-AFM signal from the Al island (bottom) connected to Au electrode shows high conductivity in HRS effectively enhancing the electric field.

Table S1: Threshold voltage (V_{th}) and the estimated active area of two-terminal Ag based devices from the literature.

Device	Geometry	Active area (μm^2)	Threshold voltage (V)	Ref.
Ag/TiO_2/Pt	Vertical	0.0007	0.3	[1]
Ag/HfO_2/Pt	Vertical	0.01	0.2	[2]
Ag/SiO_x:Ag/Pt	Vertical	0.025	0.25	[3]
Ag/HfO_x/Pd	Vertical	0.025	0.4	[4]
Ag/Ta_2O_5/Pt	Vertical	0.04	0.3	[5]
Pt/Ag:SiO_2/Pt	Vertical	0.07	0.4	[6]
Ag/SiO_2:Ag/SiO_2/Pt	Vertical	0.075	0.5	[7]
Pt/SiO_xN_y:Ag/Pt	Vertical	0.15	0.4	[8]
Ag/Ag-PVI/Pt	Vertical	0.175	0.5 – 2.6	[9]
Ag/AgI/Pt	Vertical	0.21	0.08	[10]
Ag/MoS_2/Au	Vertical	0.23	0.35 – 0.4	[11]
Ag/TiO_2/Pt	Planar	0.418	100	[12]
Ag/Mn:ZnO/Pt	Vertical	7.97	1.9	[13]
Ag/ZrO_2/Pt	Vertical	8.85	0.25	[14]
Ag/ι-carrageenan/Pt	Vertical	8.86	0.8	[15]
Au/Silk-Ag NW composite/Au	Vertical	15.4	1	[16]
Ag/SiO_2/ITO	Vertical	15.95	3	[17]
Ag/P3HT:PCBM/ITO	Vertical	22.6	1.1	[18]
Ag/WeS_2/Ag	Vertical	28	0.5	[19]
Ag/PMMA/ITO	Vertical	215	5.5	[20]
Ag/V_2C/W	Vertical	750	3.1	[21]

Ag/PVP-MoS_2 QDs/Ag	Planar	1.5×10^4	45	[22]
Au/Ag NW:TiO_2 NP/Au	Planar	2×10^4	110 – 115	[23]
Ag/Al_2O_3 NP:PI/Al	Planar	1.8×10^5	30	[24]
Au/c-Al:Ag nanostructures/Au	Planar	25×10^5	0.82	Present work

Energy consumption:

In literature for artificial synaptic devices while estimating energy consumption, the applied voltage pulse is considered analogous to the pre-synaptic spike and the resulting current change in the device is analogous to the synaptic weight change. The typical equation for the calculation of energy consumption is as follows:

$E = V_p \times I \times t_w$

where 'V_p' is the applied voltage pulse amplitude, 'I' is the corresponding current response, and 't_w' is the voltage pulse width.

While calculating energy consumption per voltage pulse in our devices, we have assumed V_p equal to the median threshold voltage (V_{th}) obtained from the DC I-V curves, the set I_{CC} as the current response of the device, and $t_w \sim 50$ m sec which is consistent throughout our studies. The current response of device D1 with voltage pulse parameters derived from IV curves is shown in Figure S13(a) as evidence. The current response for devices D2, D3, and D4 corresponding to the voltage pulse parameters derived from I-V curves was also considered in a similar manner.

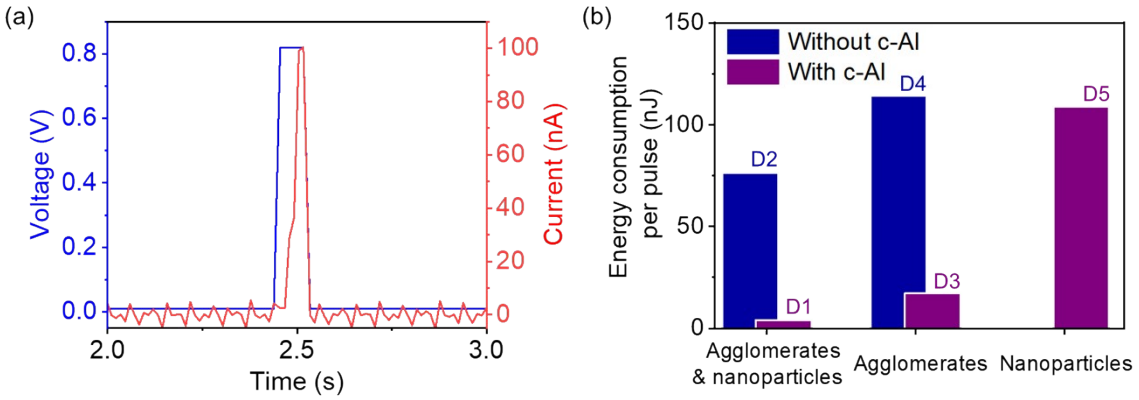

Figure S13: (a) Current response of Device D1 to the voltage pulse of V_P (V_{th}) ~ 0.82 V and t_w ~ 50 ms at the I_{CC} of 100 nA. The values were further used to calculate the energy consumption of the device. It may be noted that this value is an overestimate of the energy consumed by the device. (b) Energy consumption per applied voltage pulse as a function of different Ag configurations without and with c-Al, respectively, derived using the following formula:-

$E_{cons.} = V_{th} \times I_{CC} \times t_w$
V_{th} = median threshold voltage obtained from I-V curves
I_{CC} = 100 nA, set I_{CC}
t_w = 50 m sec, pulse width

The calculated energy consumption per pulse (few nJ) is of the whole device which contains Ag agglomerates resembling neurons, with in-between nanogaps as synaptic junction.

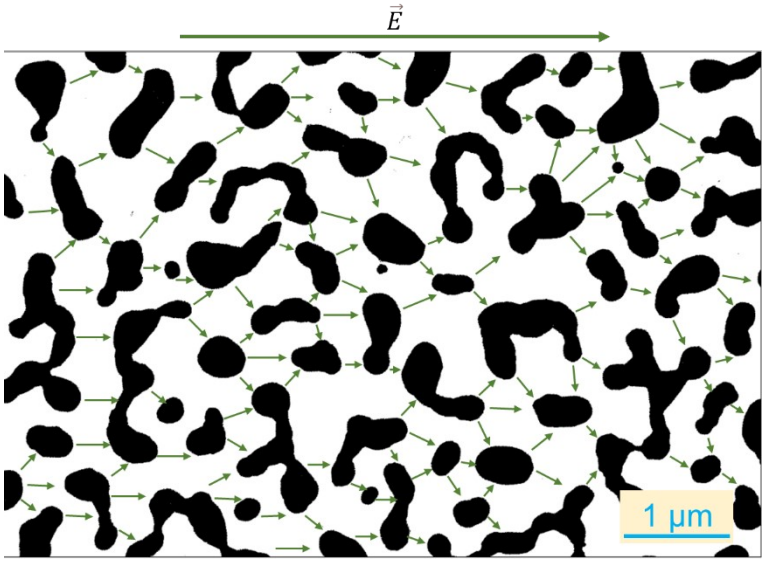

Figure S14: FESEM binary image of c-Al consisting of Ag agglomerates analysed using ImageJ software. Average agglomerate density (ρ) is found to be approx. 2 per sq. µm which is ~1.3×10^9 per sq. inch. The synapse-like junction for each agglomerate (approximately) in the direction of the electric field can vary between 2 to 4, indicated with arrow marks.

The energy consumed to form a junction between the two nearest Ag agglomerates or spatially overcome the nano-gap via electromigration is calculated using following equations:

Avg. Ag agglomerate density = ρ = agglomerate/unit area

Synapse like nanogap for each agglomerate in the direction of the electric field = n (i.e., 2 – 4)

Avg. synaptic junction density = $N = \rho \times n$

Energy consumed by a device $E_{cons.} = I_{CC} \times V_P \times t_w$

Energy density $E_0 = E_{cons.} / A$

where,

V_P = pulse voltage

I_{CC} = current compliance

t_w = pulse width

A = area of the device.

Al fill factor = f

Therefore, (1-f) = the fill factor filled with Ag agglomerates.

Actual synaptic junction density $N_0 = N \times (1\text{-}f) = \rho \times n \times (1\text{-}f)$

Energy consumed per synapse $E_s = E_0/N_0 = (I_{CC} \times V_P \times t_w / A) / (\rho \times n \times (1\text{-}f))$

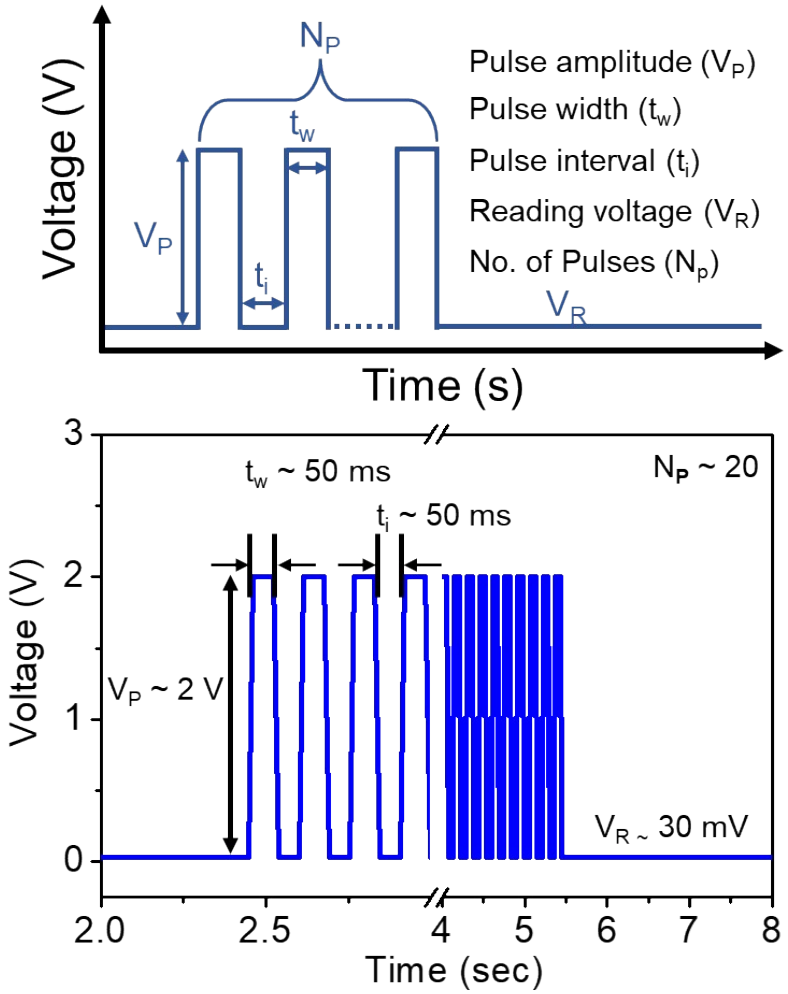

Figure S15: Schematic of the designed voltage pulse sequence and its characteristic parameters (top), actual voltage pulses applied to the device in the time domain (bottom) as an example.

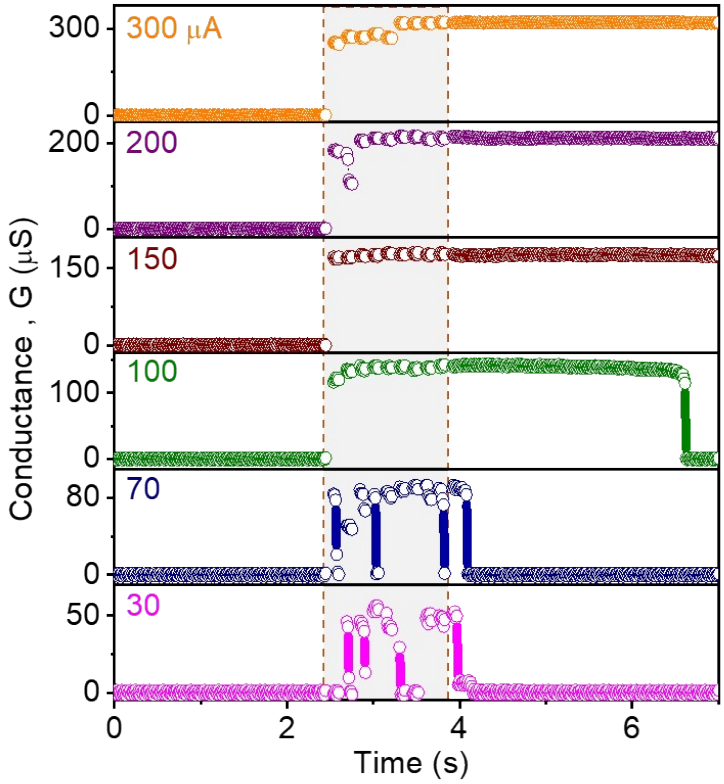

Figure S16: Time axis magnified of Fig. 3d showing Abrupt G evolution in response to voltage pulses from I_{CC} of 30 µA to 300 µA. Colour marked region denotes the pulse train timing. (V_P ~ 1V, V_R ~ 10 mV, N_P ~ 10 pulses)

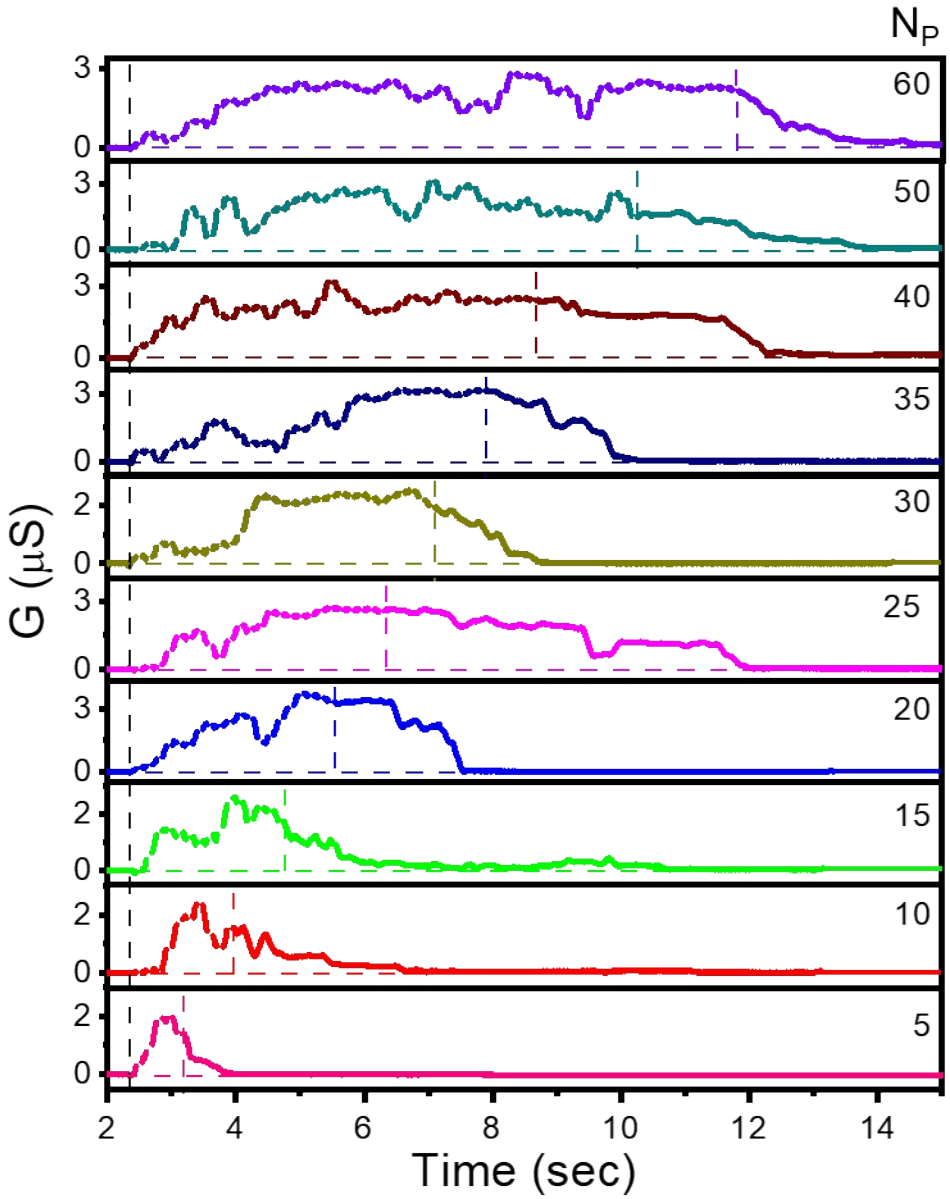

Figure S17: G profile in response to varied N_P at a low I_{CC} of 0.5 μA. Dashed lines indicate pulse train duration and N_P is mentioned on the right. (V_P ~ 2 V, V_R ~ 30 mV, t_w and t_i ~ 50 ms)

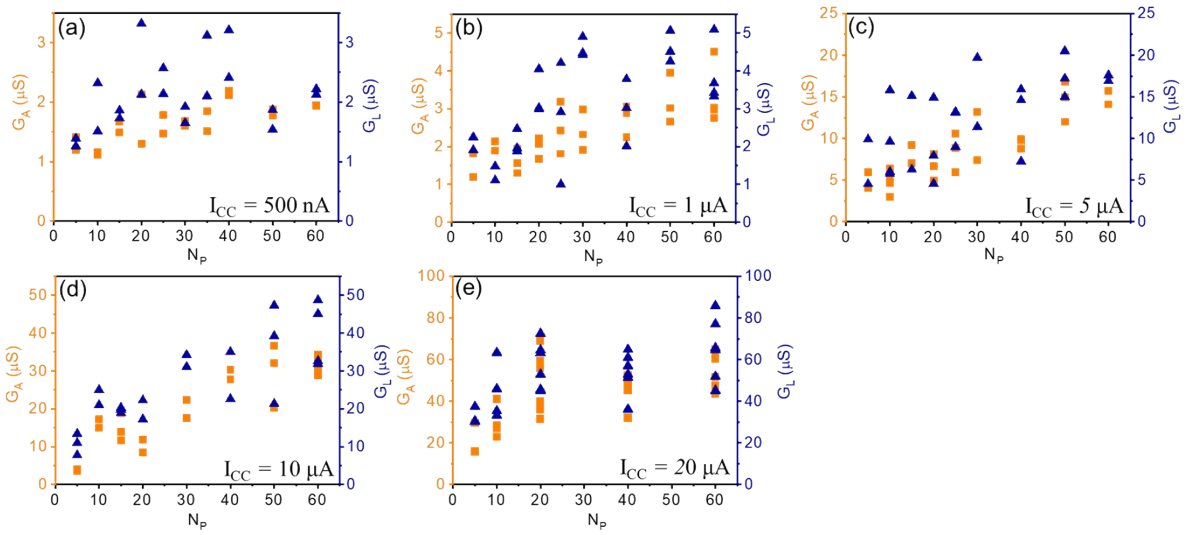

Figure S18: G_A and G_L extracted from the G profile and plotted as a function of N_P applied at the I_{CC} of (a) 500 nA, (b) 1 µA, (c) 5 µA, (d) 10 µA, and (e) 20 µA. ($V_P \sim 2V$, $V_R \sim 30$ mV, t_w and $t_i \sim 50$ ms). To avoid the discrepancy in the data points, several runs were conducted without changing any pulse parameter.

References:

1 J. Song, J. Woo, A. Prakash, D. Lee and H. Hwang, *IEEE Electron Device Lett.*, 2015, **36**, 681–683.

2 S. A. Chekol, S. Menzel, R. W. Ahmad, R. Waser and S. Hoffmann-Eifert, *Adv. Funct. Mater.*, 2022, **32**, 2111242.

3 J. H. Yoon, Z. Wang, K. M. Kim, H. Wu, V. Ravichandran, Q. Xia, C. S. Hwang and J. J. Yang, *Nat. Commun.*, 2018, **9**, 417.

4 R. Midya, Z. Wang, J. Zhang, S. E. Savel'ev, C. Li, M. Rao, M. H. Jang, S. Joshi, H. Jiang, P. Lin, K. Norris, N. Ge, Q. Wu, M. Barnell, Z. Li, H. L. Xin, R. S. Williams, Q. Xia and J. J. Yang, *Adv. Mater.*, 2017, **29**, 1604457.

5 T. Tsuruoka, T. Hasegawa, K. Terabe and M. Aono, *Nanotechnology*, 2012, **23**, 435705.

6 F. Ye, F. Kiani, Y. Huang and Q. Xia, *Adv. Mater.*, 2022, 2204778.

7 H. Jiang, D. Belkin, S. E. Savel'ev, S. Lin, Z. Wang, Y. Li, S. Joshi, R. Midya, C. Li, M. Rao, M. Barnell, Q. Wu, J. J. Yang and Q. Xia, *Nat. Commun.*, 2017, **8**, 882.

8 Z. Wang, S. Joshi, S. E. Savel'ev, H. Jiang, R. Midya, P. Lin, M. Hu, N. Ge, J. P. Strachan, Z. Li, Q. Wu, M. Barnell, G. L. Li, H. L. Xin, R. S. Williams, Q. Xia and J. J. Yang, *Nat. Mater.*, 2017, **16**, 101–108.

9 K. Krishnan and S. Vijayaraghavan, *Adv. Electron. Mater.*, 2022, **8**, 2200509.

10 S. Tappertzhofen, I. Valov and R. Waser, *Nanotechnology*, 2012, **23**, 145703.

11 D. Dev, A. Krishnaprasad, M. S. Shawkat, Z. He, S. Das, D. Fan, H. S. Chung, Y. Jung and T. Roy, *IEEE Electron Device Lett.*, 2020, **41**, 936–939.

12 C.-P. Hsiung, H.-W. Liao, J.-Y. Gan, T.-B. Wu, J.-C. Hwang, F. Chen and M.-J. Tsai, *ACS Nano*, 2010, **4**, 5414–5420.

13 Y. C. Yang, F. Pan, Q. Liu, M. Liu and F. Zeng, *Nano Lett.*, 2009, **9**, 1636–1643.

14 G. Du, C. Wang, H. Li, Q. Mao and Z. Ji, *AIP Adv.*, 2016, **6**, 085316.

15 M.-K. Kim and J.-S. Lee, *ACS Nano*, 2018, **12**, 1680–1687.

16 W. Wang, M. Wang, E. Ambrosi, A. Bricalli, M. Laudato, Z. Sun, X. Chen and D. Ielmini, *Nat. Commun.*, 2019, **10**, 1–9.

17 S. Gao, C. Chen, Z. Zhai, H. Y. Liu, Y. S. Lin, S. Z. Li, S. H. Lu, G. Y. Wang, C. Song, F. Zeng and F. Pan, *Appl. Phys. Lett.*, 2014, **105**, 063504.

18 S. Gao, F. Zeng, C. Chen, G. Tang, Y. Lin, Z. Zheng, C. Song and F. Pan, *Nanotechnology*, 2013, **24**, 335201.

19 M. Sivan, Y. Li, H. Veluri, Y. Zhao, B. Tang, X. Wang, E. Zamburg, J. F. Leong, J. X. Niu, U. Chand and A. V.-Y. Thean, *Nat. Commun.*, 2019, **10**, 5201.

20 S.-H. Lee, H.-L. Park, M.-H. Kim, M.-H. Kim, B.-G. Park and S.-D. Lee, *ACS Appl. Mater. Interfaces*, 2020, **12**, 51719–51728.

21 Y. Wang, X. Chen, D. Shen, M. Zhang, X. Chen, X. Chen, W. Shao, H. Gu, J. Xu, E. Hu, L. Wang, R. Xu and Y. Tong, *Nanomaterials*, 2021, **11**, 2860.

22 M. Li, H. An, Y. Kim, J. S. An, M. Li and T. W. Kim, *ACS Appl. Mater. Interfaces*, 2022, **14**, 44724–44734.

23 Q. Li, A. Diaz-Alvarez, R. Iguchi, J. Hochstetter, A. Loeffler, R. Zhu, Y. Shingaya, Z. Kuncic, K. Uchida and T. Nakayama, *Adv. Funct. Mater.*, 2020, **30**, 1–11.

24 C. Wu, T. W. Kim, T. Guo, F. Li, D. U. Lee and J. J. Yang, *Adv. Mater.*, 2017, **29**, 1602890.